machines

MDPI

Article

Investigation on Structural Mapping Laws of Sensitive Geometric Errors Oriented to Remanufacturing of Three-Axis Milling Machine Tools

Wenzheng Ding [1,*], Zhanqun Song [2] and Shuang Ding [2]

[1] Jiangsu Key Laboratory of Advanced Numerical Control Technology, Nanjing Institute of Technology, Nanjing 211167, China
[2] College of Mechanical Engineering, Yangzhou University, Yangzhou 225127, China; songzhanqun1@163.com (Z.S.); sding@yzu.edu.cn (S.D.)
* Correspondence: njgdsk133@126.com

Abstract: Three-axis milling machine tools are widely used in manufacturing enterprises, and they have enormous potential demands for remanufacturing to improve their performance. During remanufacturing a three-axis milling machine tool, the structure needs to be reconstructed, so it is necessary to identify sensitive geometric errors of the remanufactured machine tool. In the traditional sensitive geometric error identification method, complex error modeling and analysis must be conducted. Therefore, professional knowledge is required, and the process of the identification is cumbersome. This paper focused on the quick identification of sensitive geometric errors for remanufacturing of three-axis milling machine tools. Firstly, sensitive geometric errors of a three-axis milling machine tool were identified based on the multi-body system theory and partial differential method. Then, mapping laws between the sensitive geometric errors and the machine tool structure were firstly presented. According to the proposed mapping laws, the sensitive geometric errors can be identified quickly and easily without complex error modeling and analysis. Finally, the simulation and experiment show that the straightness error of milling is improved up to 0.007 mm by compensating the sensitive geometric errors identified by the proposed mapping laws. The table lookup method based on the mapping laws can quickly identify the sensitive geometric errors of three-axis milling machine tools, which is beneficial for the efficiency and precision of remanufacturing of machine tools.

Keywords: remanufacturing of machine tools; sensitive geometric errors; differential method; error compensation

check for updates

Citation: Ding, W.; Song, Z.; Ding, S. Investigation on Structural Mapping Laws of Sensitive Geometric Errors Oriented to Remanufacturing of Three-Axis Milling Machine Tools. *Machines* **2022**, *10*, 341. https://doi.org/10.3390/machines10050341

Academic Editor: Gianni Campatelli

Received: 21 April 2022
Accepted: 5 May 2022
Published: 6 May 2022

Publisher's Note: MDPI stays neutral with regard to jurisdictional claims in published maps and institutional affiliations.

Copyright: © 2022 by the authors. Licensee MDPI, Basel, Switzerland. This article is an open access article distributed under the terms and conditions of the Creative Commons Attribution (CC BY) license (https://creativecommons.org/licenses/by/4.0/).

1. Introduction

The worldwide market of machine tool manufacturing is approximately more than $80 billion every year. There are a large number of machine tools in service, and the quantity is still increasing because the lifetime of a machine tool is about 10 or more years. Machine tools are the most significant capital investments for manufacturing companies and represent their manufacturing capacities and technological levels. It is important to keep in-service machine tools at peak or normal performance with regular inspection and maintenance. However, with the changes of product demands, some in-service machine tools fail to meet the new machining requirements. Remanufacturing is an effective way of high resource efficiency and less downtime to upgrade in-service machine tools, instead of the purchase of new machine tools [1].

In remanufacturing of in-service machine tools, over 80% of components and parts by weight of machine tools (such as machine beds, columns and moving elements) can be reused, which can cut back on the raw materials and energy required to extract materials and process them. Remanufactured in-service machine tools can even achieve higher

performance by adding more new accessories. Three-axis milling machine tools are widely used in manufacturing enterprises, when they are remanufactured, high-precision ball screws and high performance servo motors are used instead of the original feed drive systems, and then the remanufactured three-axis milling machine tools can meet the high-precision machining requirements. To match with new machining requirements, the structure of the remanufactured three-axis machine tools needs to be redesigned and modified, and the geometric accuracy of related components and parts need to be improved.

Research showed that geometric errors of components and parts account for more than 50% of the total errors [2] and modeling, identification and compensation of geometric errors are usually used to enhance the machining accuracy of machine tools [3]. Geometric errors are commonly classified as position dependent geometric errors (PDGEs) and position independent geometric errors (PIGEs). PDGEs are mainly caused by imperfection of components, such as the straightness errors of the guide ways, while PIGEs are mainly caused by the imperfect assembly of parts, such as joint misalignments [4].

Among these geometric errors, sensitive geometric errors are the most critical errors on machining accuracy. If the sensitive geometric errors can be identified quickly according to the redesign scheme of the in-service machine tool, they can be improved accurately during remanufacturing to guarantee the machining accuracy. The key factor of the sensitive geometric error identification lies on building the mathematical model between the tool center position errors and the geometric error elements. Screw theory [5,6], multi-body system (MBS) theory [7,8], differential transform theory [3,9] and homogeneous transformation matrices (HTM) [10] are commonly used to develop geometric error model and identification model. Many scholars focused on different error analysis methods to improve the accuracy and effectiveness of sensitive error identification. The error sensitivity analysis methods are commonly categorized as local sensitivity analysis methods and global sensitivity analysis methods [11–14].

Li et al. built the geometric error model based on MBS theory of a five-axis machine tool and proposed the intuitive sensitivity indices to analyze the contributions of error components on position and posture error [13]. Similarly, the volumetric error model of a five-axis machine tool was established individually based on MBS theory, and the vital geometric errors were analyzed [14]. Li et al. modeled the geometric errors based on the multi-body system theory, and used the local sensitivity analysis method to analyze the sensitivity of errors [15]. Cheng et al. established the sensitivity matrix of a horizontal machining center based on differential transform theory and used the local sensitivity analysis method to identify the key geometric errors [16], and then adopted the Sobol global sensitivity analysis method to determine the critical geometric errors of machine tools [17]. The geometric errors affecting the uncompensatable pose accuracy were identified after the establishment of geometric error model was established, and the precision design was conducted to enhance the accuracy [18]. An improved geometric error analysis method considering the variety of sensitivities over the working space was proposed by Liu et al., and the geometric error model was established according to the MBS theory firstly [19]. In order to provide direct quantitative guidance for accuracy design of machine tools with error sensitivity analysis, Fan et al. proposed a method of error sensitivity analysis based on component incremental motion. This method can effectively identify the key parts that affect the machining accuracy of CNC machine tools [20]. Then, a quantitative interval sensitivity analysis method was developed to calculate the sensitivity of geometric errors [21]. To deal with the coupling effect of high-order error terms, a novel global method for analyzing the vital geometric error based on MBS theory and truncated Fourier expansion was proposed [22]. Guo et al. analyzed the sensitivity of PIGEs, and the results was used to optimize the compensation parameter for the accuracy improvement of a five-axis machine tool [23]. Then, the sensitive geometric errors of the rotary axis in a five-axis machine tool were investigated with Morris method and the method of gray correlation [24]. Xia et al. used the Morris global sensitivity analysis method to quantify the error sensitivity and identified the key errors and sensitive parts of a five-axis gear

profile grinding machine [25]. Li et al. established the geometric error model based on the MBS theory and the HTM firstly, and then the global maximum interval sensitivity of nine geometric error sources was extracted [26]. For coordinate measuring machines, the geometric error model of the measuring machine was established via the HTM, and then the Sobol global sensitivity analysis method is employed to study the influence of geometric errors on the measurement results [27]. Tang et al. proposed a new geometric error modeling approach based on stream of variation theory, and the new method is beneficial to identify the sensitive errors and optimize the structure configuration machine tools [28]. Aiming at the problems that the sensitivity analysis of the existing error elements was not closely related to the subsequent error compensation, Fu et al. built a geometric error contribution modeling of the motion axes, and analyzed the error sensitivity of the motion axes to find the key motion axes whose geometric errors have great influence on the accuracy of the machine tool [29]. Jiang et al. analyzed the critical geometric errors of different positions of the rotary axes by a geometric error modeling based on the MBS theory and HTM [30].

In the above literatures, to identify the sensitive geometric errors, it is needed to build individual complex error model for each kind of machine tool structure, which are unable to satisfy the rapid evaluation and comparison of several redesign schemes. Therefore, an efficient method is urgently needed to identify sensitive geometric errors directly according to the design scheme of the remanufacturing. This paper proposes a mapping law of sensitive geometric errors for remanufacturing of machine tools. The sensitive geometric errors can be recognized directly by this law according to the configuration of components and parts of remanufactured machine tools without complex modeling and sensitive analysis. The new structure scheme can be evaluated quickly according to the sensitive error terms when the remanufactured structure must be changed because of defects. Fewer sensitive items or higher components precision with sensitive items should be guaranteed. Therefore, the quick identification method, without repeated error modeling and analysis, is valuable to precision design of different machine tool structures. The proposed method is verified by simulation and experiments.

Henceforth, the rest of the paper is organized as follows: Section 2 develops the geometric error modeling of a three-axis machine tool. In Section 3, the sensitive analysis of errors is performed by partial differentiation based on the developed error model. The mapping laws between the sensitive geometric errors and structures of machine tools are summarized in Section 4. Simulation and experimental verification are carried out in Section 5. Section 6 provides the conclusions.

2. Geometric Error Modeling of a Three-Axis Machine Tool

The three-axis machine tool is a kind of in-service machine tool with the largest number, and it has enormous potential demands for remanufacturing to improve its performance. The three-axis machine is categorized in the light of configuration of axes related to the foundation, such as WXYZFT, WXYFZT, WYFXZT, and WFXYZT. The WYFXZT type is shown in Figure 1. Geometric error modeling is usually conducted according to MBS theory, where a HTM is employed to represent the transformation relationship for any two adjacent rigid bodies in the machine tool [7,8,10].

As depicted in Figure 1, six rigid bodies are included in the three-axis machine tool model, where the machine bed is selected as the foundation (F). There are two structural branches in the model. The one branch is denoted as the workpiece branch, starts from the workpiece to the machine bed (i.e., comprising the workpiece, Y-axis, and machine bed). The workpiece is supported by the Y-axis and machine bed, sequentially. The other branch is denoted as the tool branch, starts from the cutting tool to the machine bed (i.e., comprising the cutting tool, Z-axis, X-axis, and machine bed). The cutting tool is driven by the Z-axis, and the Z-axis is driven by the X-axis. The X-axis is supported by the machine bed.

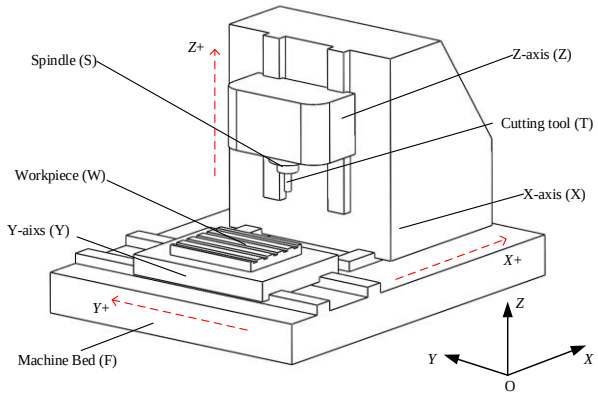


Figure 1. Structure of WYFXZT type three-axis machine tool.

From the perspective of MBS theory and rigid body kinematics, motion matrices of the model are defined as follows. When the adjacent bodies i and j are relatively static, the ideal position transformation matrix is $\boldsymbol{T}_{ijp}$, where $i \in (F, X, Y, Z)$, $j \in (X, Y, Z, W, T)$, and the position error transformation matrix is $\triangle \boldsymbol{T}_{ijp}$. When the adjacent bodies are relatively moving, the ideal position transformation matrix is $\boldsymbol{T}_{ijs}$, and the position error transformation matrix is $\triangle \boldsymbol{T}_{ijs}$. The cutting point in the tool coordinate system is represented as $[0\ 0\ 0\ 1]^{\mathrm{T}}$. Geometric error model of the machine tool shown in Figure 1 can be constructed as follows. Accordingly, the ideal position coordinate of the cutting point in the workpiece coordinate system can be expressed as Equation (1), and the actual position coordinate of the cutting point is derived as Equation (2), and thus the position error matrix is obtained by subtracting Equation (1) from Equation (2), as shown in Equation (3).

$$\boldsymbol{P}_{ideal} = (\boldsymbol{T}_{FYp}\boldsymbol{T}_{FYs}\boldsymbol{T}_{YWp}\boldsymbol{T}_{YWs})^{-1}\boldsymbol{T}_{FXp}\boldsymbol{T}_{FXs}\boldsymbol{T}_{XZp}\boldsymbol{T}_{XZs}\boldsymbol{T}_{ZTp}\boldsymbol{T}_{ZTs}\begin{bmatrix} 0 & 0 & 0 & 1 \end{bmatrix}^{\mathrm{T}} \quad (1)$$

$$\begin{aligned}\boldsymbol{P}_{actual} = {} & (\boldsymbol{T}_{FYp}\triangle\boldsymbol{T}_{FYp}\boldsymbol{T}_{FYs}\triangle\boldsymbol{T}_{FYs}\boldsymbol{T}_{YWp}\triangle\boldsymbol{T}_{YWp}\boldsymbol{T}_{YWs}\triangle\boldsymbol{T}_{YWs})^{-1}\boldsymbol{T}_{FXp}\triangle\boldsymbol{T}_{FXp}\boldsymbol{T}_{FXs}\triangle\boldsymbol{T}_{FXs}\boldsymbol{T}_{XZp} \\ & \triangle\boldsymbol{T}_{XZp}\boldsymbol{T}_{XZs}\triangle\boldsymbol{T}_{XZs}\boldsymbol{T}_{ZTp}\triangle\boldsymbol{T}_{ZTp}\boldsymbol{T}_{ZTs}\triangle\boldsymbol{T}_{ZTs}\begin{bmatrix} 0 & 0 & 0 & 1 \end{bmatrix}^{\mathrm{T}}\end{aligned} \quad (2)$$

$$\boldsymbol{E}_p = \boldsymbol{P}_{actual} - \boldsymbol{P}_{ideal} = \begin{bmatrix} \boldsymbol{E}_{px} & \boldsymbol{E}_{py} & \boldsymbol{E}_{pz} & 0 \end{bmatrix}^{\mathrm{T}} \quad (3)$$

Assuming that the posture coordinate of the tool axis in tool coordinate system is $[0\ 0\ 1\ 0]^{\mathrm{T}}$, then the ideal posture coordinate of the tool axis in the workpiece coordinate system can be expressed as Equation (4), and the actual posture coordinate of the tool axis is derived as Equation (5), and thus the posture error matrix is obtained by subtracting Equation (4) from Equation (5), as shown in Equation (6).

$$\boldsymbol{V}_{ideal} = (\boldsymbol{T}_{FYp}\boldsymbol{T}_{FYs}\boldsymbol{T}_{YWp}\boldsymbol{T}_{YWs})^{-1}\boldsymbol{T}_{FXp}\boldsymbol{T}_{FXs}\boldsymbol{T}_{XZp}\boldsymbol{T}_{XZs}\boldsymbol{T}_{ZTp}\boldsymbol{T}_{ZTs}\begin{bmatrix} 0 & 0 & 1 & 0 \end{bmatrix}^{\mathrm{T}} \quad (4)$$

$$\begin{aligned}\boldsymbol{V}_{actual} = {} & (\boldsymbol{T}_{FYp}\triangle\boldsymbol{T}_{FYp}\boldsymbol{T}_{FYs}\triangle\boldsymbol{T}_{FYs}\boldsymbol{T}_{YWp}\triangle\boldsymbol{T}_{YWp}\boldsymbol{T}_{YWs}\triangle\boldsymbol{T}_{YWs})^{-1}\boldsymbol{T}_{FXp}\triangle\boldsymbol{T}_{FXp} \\ & \boldsymbol{T}_{FXs}\triangle\boldsymbol{T}_{FXs}\boldsymbol{T}_{XZp}\triangle\boldsymbol{T}_{XZp}\boldsymbol{T}_{XZs}\triangle\boldsymbol{T}_{XZs}\boldsymbol{T}_{ZTp}\triangle\boldsymbol{T}_{ZTp}\boldsymbol{T}_{ZTs}\triangle\boldsymbol{T}_{ZTs}\begin{bmatrix} 0 & 0 & 1 & 0 \end{bmatrix}^{\mathrm{T}}\end{aligned} \quad (5)$$

$$\boldsymbol{E}_v = \boldsymbol{V}_{actual} - \boldsymbol{V}_{ideal} = \begin{bmatrix} \boldsymbol{E}_{vx} & \boldsymbol{E}_{vy} & \boldsymbol{E}_{vz} & 0 \end{bmatrix}^{\mathrm{T}} \quad (6)$$

3. Analysis of Sensitive Geometric Errors Using Partial Differentiation Method

3.1. Partial Differentiation Method

The volumetric error $\boldsymbol{E}$ includes the position error $\boldsymbol{E}_p$ and posture error $\boldsymbol{E}_v$, and it can be expressed as the function related with position coordinates.

$$\boldsymbol{E} = F(\boldsymbol{G}, \boldsymbol{W}) \quad (7)$$

There are altogether 21 geometric errors in the error model of a three-axis machine tool. Three translational errors and three angular errors associated with each axis, and

one squareness error between every two axes, and they were listed in Table 1. Therefore, in Equation (7), $\boldsymbol{G} = [\Delta x(X), \Delta x(Y), \ldots, \Delta\alpha_{yz}]$, which is the vector of 21 geometric errors; $\boldsymbol{W} = [x, y, z, 0]^T$, which is the nominal position vector of three axes.

Table 1. Definition of 21 geometric errors.

Movement Axis	Physical Meaning of Each Error Term	Symbols	Error Serial Number
X	Positioning error of the X-axis in the x direction	$\Delta x(X)$	1
	Straightness error of X-axis in y direction	$\Delta y(X)$	2
	Straightness error of X-axis in z direction	$\Delta z(X)$	3
	Rolling error of X-axis around x direction	$\Delta\alpha(X)$	4
	Angular error of X-axis around y direction	$\Delta\beta(X)$	5
	Angular error of X-axis around z direction	$\Delta\gamma(X)$	6
Y	Straightness error of Y-axis in x direction	$\Delta x(Y)$	7
	Positioning error of Y-axis in y direction	$\Delta y(Y)$	8
	Straightness error of Y-axis in z direction	$\Delta z(Y)$	9
	Angular error of Y-axis around x direction	$\Delta\alpha(Y)$	10
	Rolling error of Y-axis around y direction	$\Delta\beta(Y)$	11
	Angular error of Y-axis around z direction	$\Delta\gamma(Y)$	12
Z	Straightness error of Z-axis in x direction	$\Delta x(Z)$	13
	Straightness error of Z-axis in y direction	$\Delta y(Z)$	14
	Positioning error of Z-axis in z direction	$\Delta z(Z)$	15
	Angular error of Z-axis around x direction	$\Delta\alpha(Z)$	16
	Angular error of Z-axis around y direction	$\Delta\beta(Z)$	17
	Rolling error of Z-axis around z direction	$\Delta\gamma(Z)$	18
Assembly errors	Perpendicularity error between X-axis and Y-axis	$\Delta\gamma_{xy}$	19
	Perpendicularity error between X-axis and Z-axis	$\Delta\beta_{xz}$	20
	Perpendicularity error between Y-axis and Z-axis	$\Delta\alpha_{yz}$	21

By differentiating and ignoring the infinitesimal terms, Equation (7) can be rewritten as:

$$F(\boldsymbol{G} + \Delta\boldsymbol{G}, \boldsymbol{W} + \Delta\boldsymbol{W}) = F(\boldsymbol{G}, \boldsymbol{W}) + \frac{\partial \boldsymbol{E}}{\partial \boldsymbol{G}}\Delta\boldsymbol{G} + \frac{\partial \boldsymbol{E}}{\partial \boldsymbol{W}}\Delta\boldsymbol{W} \tag{8}$$

where, $\Delta\boldsymbol{G}$ and $\Delta\boldsymbol{W}$ are the micro increments of geometric errors and position coordinates, respectively. This paper focused on the geometric errors, hence the increments of position coordinates are assumed as zero, and thus Equation (8) can be simplified as follows.

$$F(\boldsymbol{G} + \Delta\boldsymbol{G}, \boldsymbol{W} + \Delta\boldsymbol{W}) = F(\boldsymbol{G}, \boldsymbol{W}) + \frac{\partial \boldsymbol{E}}{\partial \boldsymbol{G}}\Delta\boldsymbol{G} = \boldsymbol{E} + \Delta\boldsymbol{E} \tag{9}$$

where, $\Delta\boldsymbol{E}$ is the variation of the volumetric error $\boldsymbol{E}$ caused by the change of geometric errors of machine tools. Therefore, the analysis model of sensitivity for geometric errors can be expressed as:

$$\Delta\boldsymbol{E} = \frac{\partial \boldsymbol{E}}{\partial \boldsymbol{G}}\Delta\boldsymbol{G} = \boldsymbol{\psi}\Delta\boldsymbol{G} \tag{10}$$

where, $\boldsymbol{\psi} = \boldsymbol{\psi}_p$ or $\boldsymbol{\psi}_v$. $\boldsymbol{\psi}_p$ is the sensitivity matrix of position errors, and $\boldsymbol{\psi}_v$ is the sensitivity matrix of posture errors, as shown in Equations (11) and (12). $\boldsymbol{\psi}_p$ and $\boldsymbol{\psi}_v$ are the metrics with size 4×21, in which elements of the top three rows represent the sensitivity of 21 geometric errors in the direction of x, y and z, respectively, elements of each column represent the sensitivity of the same geometric error in the direction of x, y and z, respectively.

$$\boldsymbol{\psi}_p = \begin{bmatrix} \frac{\partial \boldsymbol{E}_{px}}{\partial \Delta x(X)} & \cdots & \frac{\partial \boldsymbol{E}_{px}}{\partial \Delta y(X)} & \cdots & \frac{\partial \boldsymbol{E}_{px}}{\partial \Delta z(X)} & \cdots & \frac{\partial \boldsymbol{E}_{px}}{\partial \Delta \beta_{xz}} & \frac{\partial \boldsymbol{E}_{px}}{\partial \Delta \alpha_{yz}} \\ \frac{\partial \boldsymbol{E}_{py}}{\partial \Delta x(X)} & \cdots & \frac{\partial \boldsymbol{E}_{py}}{\partial \Delta y(X)} & \cdots & \frac{\partial \boldsymbol{E}_{py}}{\partial \Delta z(X)} & \cdots & \frac{\partial \boldsymbol{E}_{py}}{\partial \Delta \beta_{xz}} & \frac{\partial \boldsymbol{E}_{py}}{\partial \Delta \alpha_{yz}} \\ \frac{\partial \boldsymbol{E}_{pz}}{\partial \Delta x(X)} & \cdots & \frac{\partial \boldsymbol{E}_{pz}}{\partial \Delta y(X)} & \cdots & \frac{\partial \boldsymbol{E}_{pz}}{\partial \Delta z(X)} & \cdots & \frac{\partial \boldsymbol{E}_{pz}}{\partial \Delta \beta_{xz}} & \frac{\partial \boldsymbol{E}_{pz}}{\partial \Delta \alpha_{yz}} \\ 0 & \ldots & 0 & \ldots & 0 & \ldots & 0 & 0 \end{bmatrix} \tag{11}$$

$$\boldsymbol{\psi}_v = \begin{bmatrix} \frac{\partial \boldsymbol{E}_{vx}}{\partial \Delta x(X)} & \cdots & \frac{\partial \boldsymbol{E}_{vx}}{\partial \Delta y(X)} & \cdots & \frac{\partial \boldsymbol{E}_{vx}}{\partial \Delta z(X)} & \cdots & \frac{\partial \boldsymbol{E}_{vx}}{\partial \Delta \beta_{xz}} & \frac{\partial \boldsymbol{E}_{vx}}{\partial \Delta \alpha_{yz}} \\ \frac{\partial \boldsymbol{E}_{vy}}{\partial \Delta x(X)} & \cdots & \frac{\partial \boldsymbol{E}_{vy}}{\partial \Delta y(X)} & \cdots & \frac{\partial \boldsymbol{E}_{vy}}{\partial \Delta z(X)} & \cdots & \frac{\partial \boldsymbol{E}_{vy}}{\partial \Delta \beta_{xz}} & \frac{\partial \boldsymbol{E}_{vy}}{\partial \Delta \alpha_{yz}} \\ \frac{\partial \boldsymbol{E}_{vz}}{\partial \Delta x(X)} & \cdots & \frac{\partial \boldsymbol{E}_{vz}}{\partial \Delta y(X)} & \cdots & \frac{\partial \boldsymbol{E}_{vz}}{\partial \Delta z(X)} & \cdots & \frac{\partial \boldsymbol{E}_{vz}}{\partial \Delta \beta_{xz}} & \frac{\partial \boldsymbol{E}_{vz}}{\partial \Delta \alpha_{yz}} \\ 0 & \ldots & 0 & \ldots & 0 & \ldots & 0 & 0 \end{bmatrix} \tag{12}$$

3.2. An Example to Analyze the Sensitivity of a Machine Tool

According to Equations (11) and (12), the sensitivity matrix of position errors for the structure illustrated in Figure 1 can be expressed as:

$$\boldsymbol{\psi}_p = \begin{bmatrix} 1 & 0 & 0 & 0 & z & 0 & -1 & 0 & 0 & 0 & -z & -y & 1 & 0 & 0 & 0 & 0 & 0 & 0 & z & 0 \\ 0 & 1 & 0 & -z & 0 & 0 & 0 & -1 & 0 & z & 0 & -x & 0 & 1 & 0 & 0 & 0 & 0 & x & 0 & -z \\ 0 & 0 & 1 & 0 & 0 & 0 & 0 & 0 & -1 & y & x & 0 & 0 & 0 & 1 & 0 & 0 & 0 & 0 & 0 & 0 \\ 0 & 0 & 0 & 0 & 0 & 0 & 0 & 0 & 0 & 0 & 0 & 0 & 0 & 0 & 0 & 0 & 0 & 0 & 0 & 0 & 0 \end{bmatrix} \tag{13}$$

The sensitivity matrix of posture errors for the structure illustrated in Figure 1 can be expressed as:

$$\boldsymbol{\psi}_v = \begin{bmatrix} 0 & 0 & 0 & 0 & 1 & 0 & 0 & 0 & 0 & 0 & -1 & 0 & 0 & 0 & 0 & 0 & 1 & 0 & 0 & 1 & 0 \\ 0 & 0 & 0 & -1 & 0 & 0 & 0 & 0 & 0 & 1 & 0 & 0 & 0 & 0 & 0 & -1 & 0 & 0 & 0 & 0 & -1 \\ 0 & 0 & 0 & 0 & 0 & 0 & 0 & 0 & 0 & 0 & 0 & 0 & 0 & 0 & 0 & 0 & 0 & 0 & 0 & 0 & 0 \\ 0 & 0 & 0 & 0 & 0 & 0 & 0 & 0 & 0 & 0 & 0 & 0 & 0 & 0 & 0 & 0 & 0 & 0 & 0 & 0 & 0 \end{bmatrix} \tag{14}$$

The motion stroke of X, Y and Z axes of structure in Figure 1 are 500 mm, 350 mm and 450 mm, respectively, and the most common work range is from 100 mm to 200 mm for each axis. In the cube workspace, 9 points are selected, as illustrated in Figure 2. Taking point P1 as an example, its sensitivity matrix of position error is represented as Equation (15), and its sensitivity matrix of posture error is represented as Equation (16).

$$\boldsymbol{\psi}_{p_1} = \begin{bmatrix} 1 & 0 & 0 & 0 & 0.1 & 0 & -1 & 0 & 0 & 0 & -0.1 & -0.1 & 1 & 0 & 0 & 0 & 0 & 0 & 0 & 0.1 & 0 \\ 0 & 1 & 0 & -0.1 & 0 & 0 & 0 & -1 & 0 & 0.1 & 0 & -0.1 & 0 & 1 & 0 & 0 & 0 & 0 & 0.1 & 0 & -0.1 \\ 0 & 0 & 1 & 0 & 0 & 0 & 0 & 0 & -1 & 0.1 & 0.1 & 0 & 0 & 0 & 1 & 0 & 0 & 0 & 0 & 0 & 0 \\ 0 & 0 & 0 & 0 & 0 & 0 & 0 & 0 & 0 & 0 & 0 & 0 & 0 & 0 & 0 & 0 & 0 & 0 & 0 & 0 & 0 \end{bmatrix} \tag{15}$$

$$\boldsymbol{\psi}_{v_1} = \begin{bmatrix} 0 & 0 & 0 & 0 & 1 & 0 & 0 & 0 & 0 & 0 & -1 & 0 & 0 & 0 & 0 & 0 & 1 & 0 & 0 & 1 & 0 \\ 0 & 0 & 0 & -1 & 0 & 0 & 0 & 0 & 0 & 1 & 0 & 0 & 0 & 0 & 0 & -1 & 0 & 0 & 0 & 0 & -1 \\ 0 & 0 & 0 & 0 & 0 & 0 & 0 & 0 & 0 & 0 & 0 & 0 & 0 & 0 & 0 & 0 & 0 & 0 & 0 & 0 & 0 \\ 0 & 0 & 0 & 0 & 0 & 0 & 0 & 0 & 0 & 0 & 0 & 0 & 0 & 0 & 0 & 0 & 0 & 0 & 0 & 0 & 0 \end{bmatrix} \tag{16}$$

Similarly, the sensitivity metrics of other eight points can be obtained by the same way. Figures 3–5 show the sensitivity index of position error on 21 geometric errors for nine points in the x, y, and z direction, respectively, and the horizontal coordinates represent the error serial number in Table 1. Figures 6 and 7 illustrate the sensitivity index of posture error on 21 geometric errors for nine points in the x and y direction, respectively. The sensitivity indices of posture error on 21 geometric errors for nine points in the direction of z are all equal to zero.

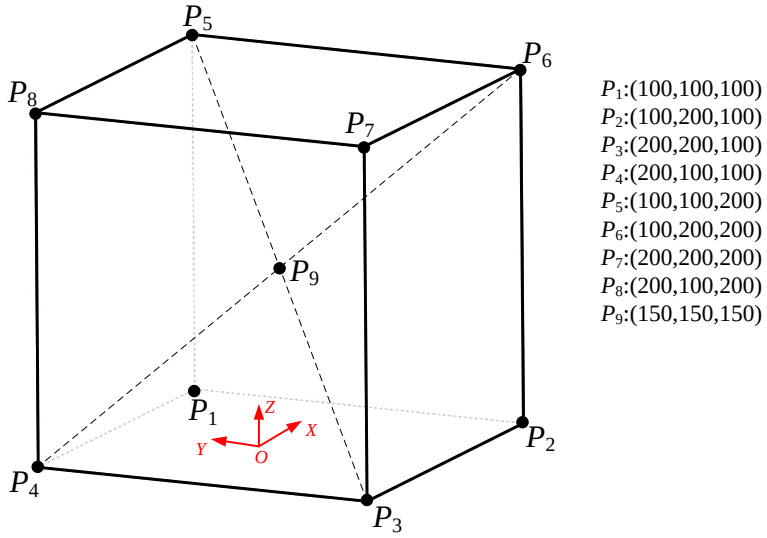


Figure 2. Location schematic diagram of the analysis point in the workspace.

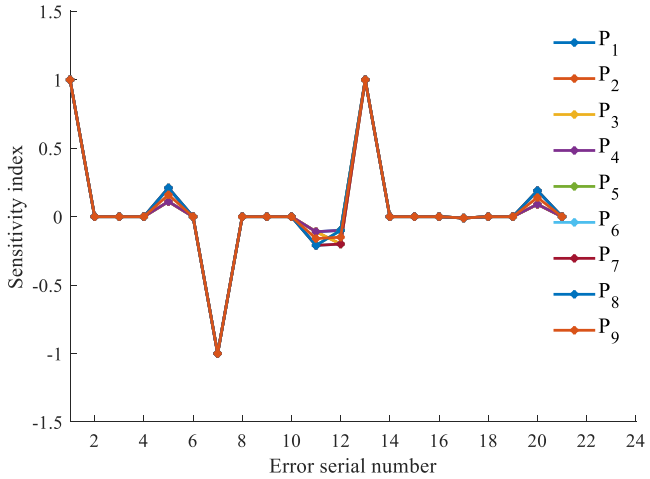


Figure 3. Sensitivity index of position errors in the x direction.

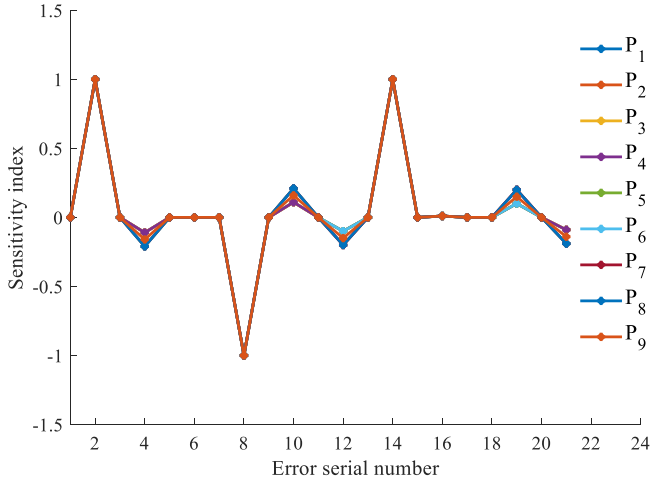


Figure 4. Sensitivity index of position error in the y direction.

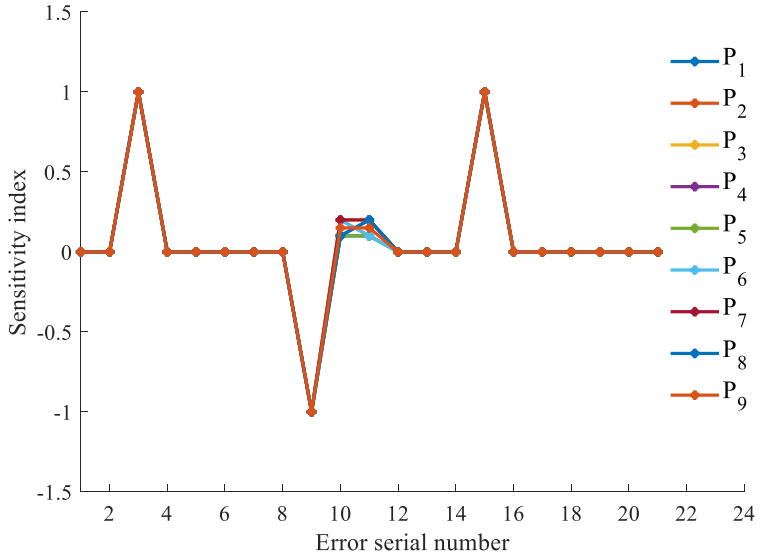


Figure 5. Sensitivity index of position error in the z direction.

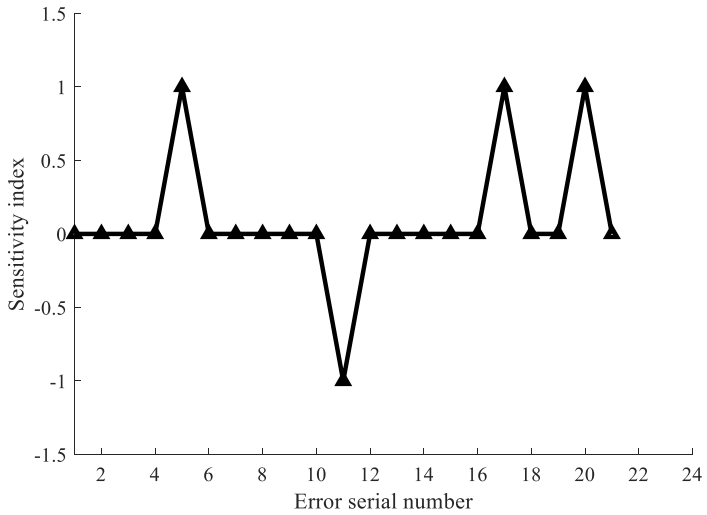


Figure 6. Sensitivity index of posture error in the x direction.

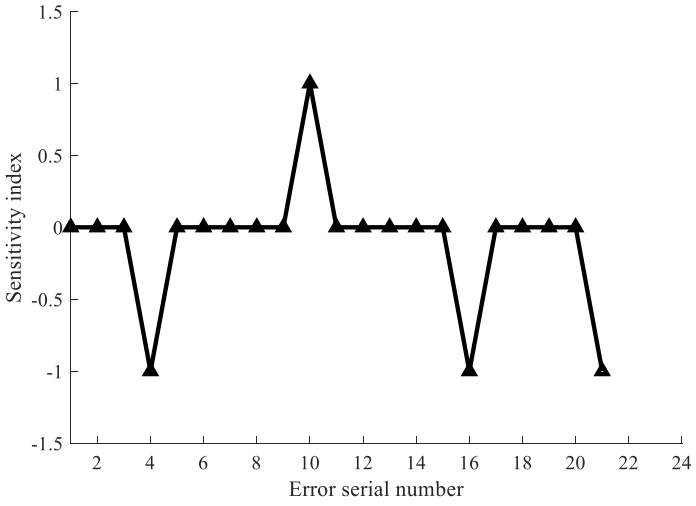


Figure 7. Sensitivity index of posture error in the y direction.

4. Mapping Law between Sensitive Geometric Errors and the Structure of a Three-Axis Remanufactured Machine Tool

The correlation between sensitive errors and configuration structure of machine tools is analyzed by the calculation method of sensitive geometric errors described in Section 3. The correlation law between sensitive geometric errors and the structure of a three-axis remanufactured machine tool is systematically summarized according to the classification of linear error, angular error, PDGEs and PIGEs, as shown in Figure 8.

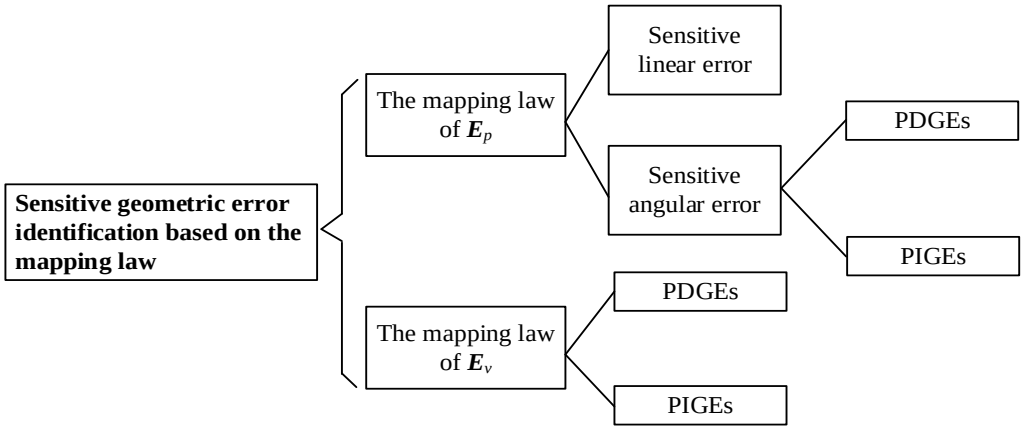


Figure 8. Sensitive geometric error identification process based on the proposed mapping law.

The error identification direction mentioned in this paper is x, y and z direction, respectively, which denote the x, y and z direction of volume error that consistent with the X, Y and Z axis of the machine tool. The linear errors with prefix Δx, Δy, Δz are the deviations along with the X, Y and Z axis, respectively. The angular errors with prefix $\Delta\alpha$, $\Delta\beta$, and $\Delta\gamma$ are the angles rotated around the X, Y and Z axis, respectively.

4.1. Mapping Law between Sensitive Geometric Errors of Volumetric Position Error and the Structure

The mapping laws between sensitive geometric errors of volumetric position error and the structure of the three-axis machine tool are summarized in this section. The sensitive geometric errors are identified in x, y and z direction by using the mapping laws, respectively. The mapping laws are described according to the machine tool structure shown in Figure 1.

The geometric errors of the machine tool are categorized as linear error and angular error. The topological motion chain of the machine tool is determined firstly. Then, the mapping laws are expressed according to the two categories of sensitive linear error and sensitive angular error. Taking the machine structure shown in Figure 1 as an example, the workpiece chain is "Machine Bed—Y-axis—Workpiece" and the tool chain is "Machine Bed—X-axis—Z-axis—Spindle—Cutting Tool", respectively. The mapping laws of volumetric position error were listed as the mapping table, seen in Table 2.

4.1.1. Mapping Law of Sensitive Linear Error

The linear errors of all axes in the corresponding identification direction are the sensitive errors. The sensitive linear errors in x direction are $\Delta x(X)$, $\Delta x(Y)$, and $\Delta x(Z)$, the sensitive linear errors in y direction are $\Delta y(X)$, $\Delta y(Y)$, and $\Delta y(Z)$, and the sensitive linear errors in the z direction are $\Delta z(X)$, $\Delta z(Y)$, and $\Delta z(Z)$, respectively.

Table 2. Identification law of sensitive geometric errors of volumetric position error.

Identification Direction	Sensitive Geometric Errors of Volumetric Position Error													
	Sensitive Linear Error	Sensitive Angular Errors												
		PDGEs						PIGEs						
		Workpiece Chain			Tool Chain			Motion Axis Next to the Workpiece			Motion Axis Next to the Tool			The Third Motion Axis
		If There Is No Motion Axis on the Corresponding Chain, the Corresponding PDGEs Are Removed												
		X	Y	Z	Direction of Cutter Axis x	y	z	X	Y	Z	X	Y	Z	
x	$\Delta x(X)$ $\Delta x(Y)$ $\Delta x(Z)$	$\Delta\beta(X)$ $\Delta\gamma(X)$	$\Delta\beta(Y)$ $\Delta\gamma(Y)$	$\Delta\beta(Z)$ $\Delta\gamma(Z)$	- -	$\Delta\gamma(X)$ $\Delta\gamma(Y)$ $\Delta\gamma(Z)$	$\Delta\beta(X)$ $\Delta\beta(Y)$ $\Delta\beta(Z)$	$\Delta\beta_{xz}$ $\Delta\gamma_{xy}$			- -			The sensitive angular PIGEs in the third direction of motion axis is the squareness error that not appeared in the direction of motion axis next to the workpiece. For example: if X-axis is next to the workpiece, the sensitive angular PIGEs in the third direction is $\Delta\alpha_{yz}$.
y	$\Delta y(X)$ $\Delta y(Y)$ $\Delta y(Z)$	$\Delta\alpha(X)$ $\Delta\gamma(X)$	$\Delta\alpha(Y)$ $\Delta\gamma(Y)$	$\Delta\alpha(Z)$ $\Delta\gamma(Z)$	$\Delta\gamma(X)$ $\Delta\gamma(Y)$ $\Delta\gamma(Z)$	- -	$\Delta\alpha(X)$ $\Delta\alpha(Y)$ $\Delta\alpha(Z)$		$\Delta\alpha_{yz}$ $\Delta\gamma_{xy}$			- -		
z	$\Delta z(X)$ $\Delta z(Y)$ $\Delta z(Z)$	$\Delta\alpha(X)$ $\Delta\beta(X)$	$\Delta\alpha(Y)$ $\Delta\beta(Y)$	$\Delta\alpha(Z)$ $\Delta\beta(Z)$	$\Delta\beta(X)$ $\Delta\beta(Y)$ $\Delta\beta(Z)$	$\Delta\alpha(X)$ $\Delta\alpha(Y)$ $\Delta\alpha(Z)$	- -			$\Delta\alpha_{yz}$ $\Delta\beta_{xz}$			- -	

4.1.2. Mapping Law of Sensitive Angular Error

The mapping laws of sensitive angular error are expressed according to the classification of PDGEs and PIGEs.

(1) Mapping law to identify sensitive angular PDGEs

a. Sensitive angular PDGEs identification of motion axis on workpiece chain. Each moving axis on workpiece chain has two sensitive angular PDGEs in the corresponding identification direction. The two errors are the angular errors around another two directions in addition to the identification direction. The sensitive angular PDGEs of the X-axis, Y-axis and Z-axis can be identified as follows: The sensitive angular PDGEs of the X-axis in the x identification direction on workpiece chain are $\Delta\beta(X)$, $\Delta\gamma(X)$. The sensitive angular PDGEs of the Y-axis in the x identification direction on workpiece chain are $\Delta\beta(Y)$ and $\Delta\gamma(Y)$. The sensitive angular PDGEs of the Z-axis in the x identification direction on workpiece chain are $\Delta\beta(Z)$ and $\Delta\gamma(Z)$. The sensitive angular PDGEs of the X-axis in the y identification direction on workpiece chain are $\Delta\alpha(X)$ and $\Delta\gamma(X)$. The sensitive angular PDGEs of the Y-axis in the y identification direction on workpiece chain are $\Delta\alpha(Y)$ and $\Delta\gamma(Y)$. The sensitive angular PDGEs of the Z-axis in the y identification direction on workpiece chain are $\Delta\alpha(Z)$ and $\Delta\gamma(Z)$. The sensitive angular PDGEs of the X-axis in the z identification direction on workpiece chain are $\Delta\alpha(X)$ and $\Delta\beta(X)$. The sensitive angular PDGEs of the Y-axis in the z identification direction on workpiece chain are $\Delta\alpha(Y)$ and $\Delta\beta(Y)$. The sensitive angular PDGEs of the Z-axis in the z identification direction on workpiece chain are $\Delta\alpha(Z)$ and $\Delta\beta(Z)$

b. Sensitive angular PDGEs identification of motion axis on tool chain The relationship between the identification direction and the direction of cutter axis will affect the mapping law. If the identification direction is accordance with the direction of cutter axis. There are no sensitive angular PDGEs in the identification direction of all axes on the tool chain. As shown in Figure 1, the cutter

axis is along with z direction, hence X-axis and Z-axis on the tool chain have no sensitive angular PDGEs in the identification z direction. If the identification direction is inconsistent with the cutter axis direction. Each motion axis on the tool chain has one sensitive angular PDGEs. The sensitive angular PDGEs rotated around the third axis except the identification direction and the cutter axis direction. See in Figure 1, the cutter axis is along with z direction, hence the sensitive angular PDGEs in x identification direction are $\Delta\beta(X)$ and $\Delta\beta(Z)$, the sensitive angular PDGEs in y identification direction are $\Delta\alpha(X)$ and $\Delta\alpha(Z)$.

(2) Mapping law to identify sensitive angular PIGEs

a. The identification direction consistent with the direction of motion axis next to the workpiece has two sensitive angular PIGEs. Squareness errors between the motion axis and the other two axes are the sensitive angular PIGEs. As shown in Figure 1, Y-axis is next to the workpiece, hence $\Delta\gamma_{xy}$ and $\Delta\alpha_{yz}$ are the sensitive angular PIGEs in the y direction.

b. There are no sensitive angular PIGEs in the identification direction consistent with the motion axis next to the tool. As shown in Figure 1, Z-axis is next to the tool on the tool chain, hence there are no sensitive angular PIGEs in the z direction.

c. The last one sensitive angular PIGE can be found in the remaining third identification direction. As shown in Figure 1, Y-axis is closest to the workpiece, and Z-axis is closest to the tool. Hence, the x identification direction corresponding to the remaining X-axis has a sensitive angular PIGE $\Delta\beta_{xz}$

4.2. Mapping Law between Sensitive Geometric Errors of Volumetric Posture Error and the Structure

It is well known that the linear errors have no influence on the posture error of the volumetric posture error. Therefore, the mapping law of volumetric posture error is divided into angular PDGEs and PIGEs. Similarly, the mapping laws of volumetric posture error were listed as the mapping table, shown in Table 3.

Table 3. Identification law of sensitive geometric errors of volumetric posture error.

Identification Direction	**Sensitive Geometric Errors of Volumetric Posture Error**					
	PDGEs			**PIGEs**		
	Direction of Cutter Axis			**Direction of Cutter Axis**		
	x	**y**	**z**	**x**	**y**	**z**
x	- -	$\Delta\gamma(X)$ $\Delta\gamma(Y)\Delta\gamma(Z)$	$\Delta\beta(X)$ $\Delta\beta(Y)\Delta\beta(Z)$	- -	$\Delta\gamma_{xy}$	$\Delta\beta_{xz}$
y	$\Delta\gamma(X)$ $\Delta\gamma(Y)\Delta\gamma(Z)$	- -	$\Delta\alpha(X)$ $\Delta\alpha(Y)\Delta\alpha(Z)$	$\Delta\gamma_{xy}$	- -	$\Delta\alpha_{yz}$
z	$\Delta\beta(X)$ $\Delta\beta(Y)\Delta\beta(Z)$	$\Delta\alpha(X)$ $\Delta\alpha(Y)\Delta\alpha(Z)$	- -	$\Delta\beta_{xz}$	$\Delta\alpha_{yz}$	- -

(1) Mapping law to identify sensitive angular PDGEs

The relationship between the identification direction and the direction of cutter axis will affect the mapping law.

If the identification direction is accordance with the direction of cutter axis. There are no sensitive angular PDGEs in the identification direction of all axes. As shown in Figure 1, the cutter axis is along with z direction, hence X-axis, Y-axis and Z-axis have no sensitive angular PDGEs in the identification z direction.

If the identification direction is inconsistent with the cutter axis direction. Each motion axis has one sensitive angular PDGEs. The sensitive angular PDGEs rotated around the third axis except the identification direction and the cutter axis direction. As shown in Figure 1, the cutter axis is along with z direction, hence the sensitive angular PDGEs in

x identification direction are $\Delta\beta(X)$, $\Delta\beta(Y)$ and $\Delta\beta(Z)$, the sensitive angular PDGEs in y identification direction are $\Delta\alpha(X)$, $\Delta\alpha(Y)$ and $\Delta\alpha(Z)$.

(2) Mapping law to identify sensitive angular PIGEs

Similarly, the mapping law of sensitive PIGEs are also discussed according to the two cases that the identification direction is in the same direction with cutter axis direction and the identification direction is different from cutter axis direction.

If the identification direction is accordance with the direction of cutter axis. There are no sensitive angular PIGEs in the identification direction of all axes.

If the identification direction is inconsistent with the cutter axis direction. One sensitive angular PIGE can be found in each identification direction. The sensitive PIGE is the squareness error between the identification direction and the cutter axis direction. As shown in Figure 1, the cutter axis is along with z direction, hence the sensitive PIGE in the x direction is $\Delta\beta_{xz}$, and the sensitive PIGE in the y direction is $\Delta\alpha_{yz}$.

5. Simulation and Experiments

5.1. Quick Identification of Geometric Errors Based on the Mapping Table

Identification of sensitive geometric errors for another structure of an orthogonal three-axis machine tool, shown in Figure 9, was conducted according to the mapping law presented in Section 4.1. and 4.2. The workpiece chain of the machine tool is "Machine Bed—X-axis—Y-axis—Workpiece", and the tool chain is "Machine bed—Z-axis—Spindle—Cutting Tool". The sensitive geometric errors of volumetric position error and posture error can be easily obtained according to the structure chain and the mapping law as shown in Tables 2 and 3.

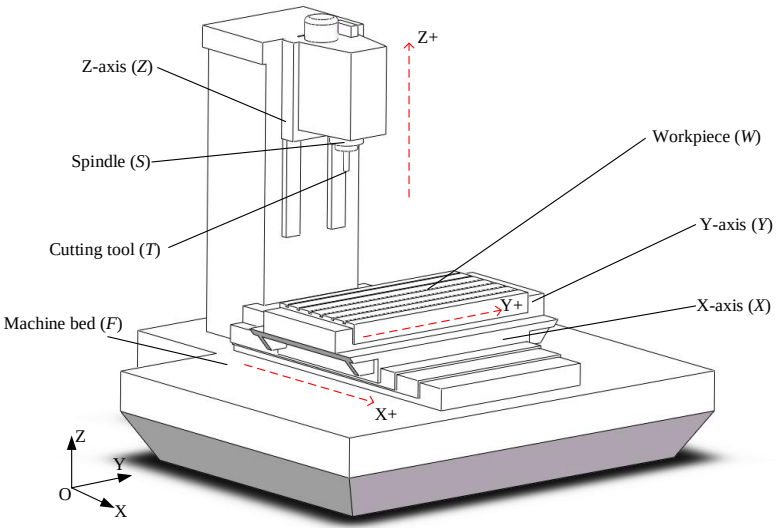


Figure 9. Structural diagram of another WYXFZT type three-axis machine tool.

Firstly, sensitive geometric errors of volumetric position error are identified. Sensitive linear errors in x, y, and z direction are not affected by the structure, therefore, the error elements of the 'Sensitive linear error' column remain unchanged as in Table 2. X-axis and Y-axis can be found in the Workpiece chain, see in Figure 9. Hence, the PDGE elements of the corresponding X-axis and Y-axis in 'Workpiece chain' column are reserved, as listed in Table 2. Additionally, the PDGE elements of the Z-axis in 'Workpiece chain' column were deleted. Z-axis is found in the tool chain, and the cutter axis direction is accordance with the z direction. Therefore, the PDGEs of Z-axis, $\Delta\beta(Z)$ and $\Delta\alpha(Z)$, in the third 'Tool chain' column should be retained.

For the identification of sensitive PIGEs, Y-axis is found next to the workpiece, see in Figure 9. Therefore, the corresponding Y column of the 'Motion axis next to the Workpiece' column is retained, as listed in Table 4. $\Delta\alpha_{yz}$ and $\Delta\gamma_{xy}$ are the sensitive PIGEs in the

y direction. There are no sensitive PIGEs in z direction because Z-axis is found next to the tool. The third direction is x direction, and the last PIGEs $\Delta\beta_{xz}$ is identified as the sensitive PIGEs in x direction. All the sensitive PDGEs and PIGEs in x, y, and z direction can be identified, respectively. The identified results are listed in Table 4. According to the structure in Figure 9, principle of the identification method proposed in this paper can be discovered by comparing Table 4 to Table 2. Similarly, the identified results of volumetric posture error are listed in Table 5 according to Table 3. Dramatically, Table 4 contains all sensitive error items that listed in Table 5.

Table 4. Sensitive geometric errors of volumetric position error of structure shown in Figure 9 based on Table 2.

Identification Direction	Sensitive Geometric Errors of Volumetric Position Error						
	Sensitive Linear Error	Sensitive Angular Errors					
		PDGEs			PIGEs		
		Workpiece Chain		Tool Chain	Motion Axis Next to the Workpiece	Motion Axis Next to the Tool	The Third Motion Axis
		If There Is No Motion Axis on the Corresponding Chain, the Corresponding PDGEs Are Removed					
		X	Y	Direction of Cutter Axis z	Y	Z	
x	$\Delta x(X)$ $\Delta x(Y)$ $\Delta x(Z)$	$\Delta\beta(X)$ $\Delta\gamma(X)$	$\Delta\beta(Y)$ $\Delta\gamma(Y)$	$\Delta\beta(Z)$			$\Delta\beta_{xz}$
y	$\Delta y(X)$ $\Delta y(Y)$ $\Delta y(Z)$	$\Delta\alpha(X)$ $\Delta\gamma(X)$	$\Delta\alpha(Y)$ $\Delta\gamma(Y)$	$\Delta\alpha(Z)$	$\Delta\alpha_{yz}$ $\Delta\gamma_{xy}$		
z	$\Delta z(X)$ $\Delta z(Y)$ $\Delta z(Z)$	$\Delta\alpha(X)$ $\Delta\beta(X)$	$\Delta\alpha(Y)$ $\Delta\beta(Y)$	–		–	

Table 5. Sensitive geometric errors of volumetric posture error of structure in Figure 9 based on Table 3.

Identification Direction	Sensitive Geometric Errors of Volumetric Posture Error	
	PDGEs	PIGEs
	Direction of Cutter Axis	Direction of Cutter Axis
	z	z
x	$\Delta\beta(X)\Delta\beta(Y)\Delta\beta(Z)$	$\Delta\beta_{xz}$
y	$\Delta\alpha(X)\Delta\alpha(Y)\Delta\alpha(Z)$	$\Delta\alpha_{yz}$
z	–	–

5.2. Simulation Verification

It is well known that the posture error cannot be compensated well with no rotary axis of a three-axis machine tool. The sensitive angular errors should be paid more attention during the redesign and reassembling of remanufactured three-axis machine tools. Therefore, only the volumetric position error is analyzed before and after compensation in this section. The forward kinematics model considering geometric errors of the WYXFZT type three-axis machine tool, see in Figure 9, was built according to the MBS theory and HTM, the results are displayed as follows:

$$\begin{bmatrix} x_w & y_w & z_w & 1 \end{bmatrix}^{\mathrm{T}} = (\boldsymbol{T}_{FXp}\Delta\boldsymbol{T}_{FXp}\boldsymbol{T}_{FXs}\Delta\boldsymbol{T}_{FXs}\boldsymbol{T}_{XYp}\Delta\boldsymbol{T}_{XYp}\boldsymbol{T}_{XYs}\Delta\boldsymbol{T}_{XYs}\boldsymbol{T}_{YWp}\Delta\boldsymbol{T}_{YWp}\boldsymbol{T}_{YWs}\Delta\boldsymbol{T}_{YWs})^{-1} \boldsymbol{T}_{FZp}\Delta\boldsymbol{T}_{FZp}\boldsymbol{T}_{FZs}\Delta\boldsymbol{T}_{FZs}\boldsymbol{T}_{ZTp}\Delta\boldsymbol{T}_{ZTp}\boldsymbol{T}_{ZTs}\Delta\boldsymbol{T}_{ZTs}\begin{bmatrix} 0 & 0 & 0 & 1 \end{bmatrix}^{\mathrm{T}} \quad (17)$$

where x_w, y_w, z_w are the cutter locations in the workpiece coordinate system. The analytical expressions of geometric error compensation can be derived based on the actual inverse kinematics [10]. Then, the motion value of motion axis after error compensation can be

calculated directly according to the geometric errors and cutter location (CL) data by using the analytical expressions. Expanding Equation (17) from matrix format to polynomial format. Then, the analytical expressions after error compensation can be solved according to Equation (17):

$$\begin{cases} X = -x_w - \Delta x(X) - \Delta x(Y) + \Delta x(Z) + \Delta\gamma(Y)y_w - (\Delta\beta(X) + \Delta\beta(Y) - \Delta\beta_{xz})z_w \\ Y = -y_w - \Delta y(X) - \Delta y(Y) + \Delta y(Z) - (\Delta\gamma(X) + \Delta\gamma_{xy})x_w + (\Delta\alpha(X) + \Delta\alpha(Y) - \Delta\alpha_{yz})z_w \\ Z = z_w + \Delta z(X) + \Delta z(Y) - \Delta z(Z) - (\Delta\beta(X) + \Delta\beta(Y))x_w + \Delta\alpha(Y)y_w \end{cases} \quad (18)$$

With considering the geometric errors, Equation (18) gives the relationship between the modified motion commands and the CLs. The corrected numerical control commands of X-axis, Y-axis and Z-axis can be calculated by substituting the CLs and geometric errors into Equation (18). Then, the geometric errors are compensated by using the corrected motion commands.

The linear PDGEs in the simulation were set as 0.01 mm × sin(0.5 × position) and the angular PDGEs were set as 0.01 deg × sin(0.5 × position). The angular PIGEs of three-axis machine tools were set as 0.01 deg. Then, 110 points of a NAS piece were selected to verify the correctness of identification results of sensitive errors, as shown in Figure 10.

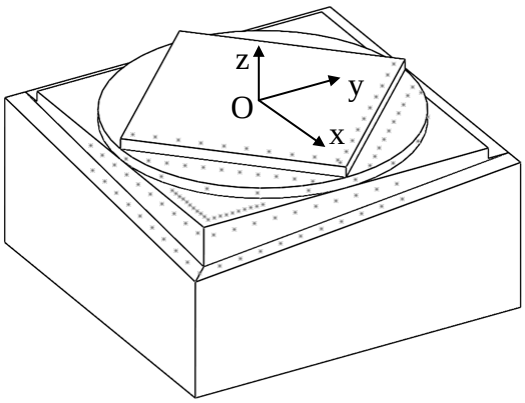
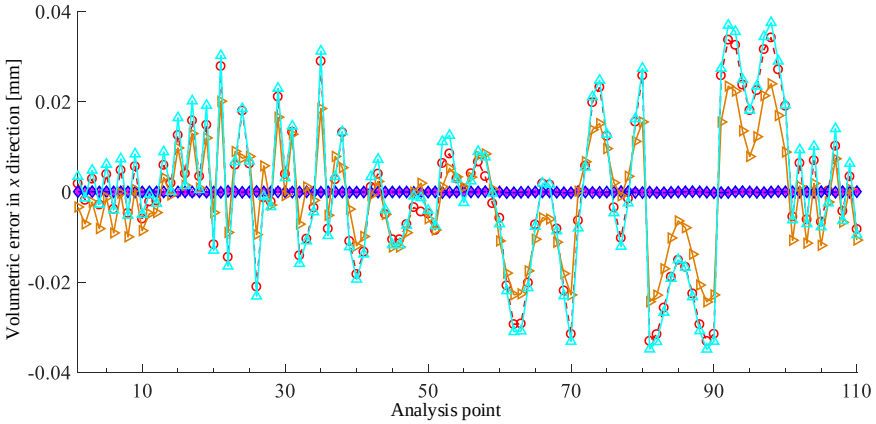


Figure 10. Simulation points on the NAS piece.

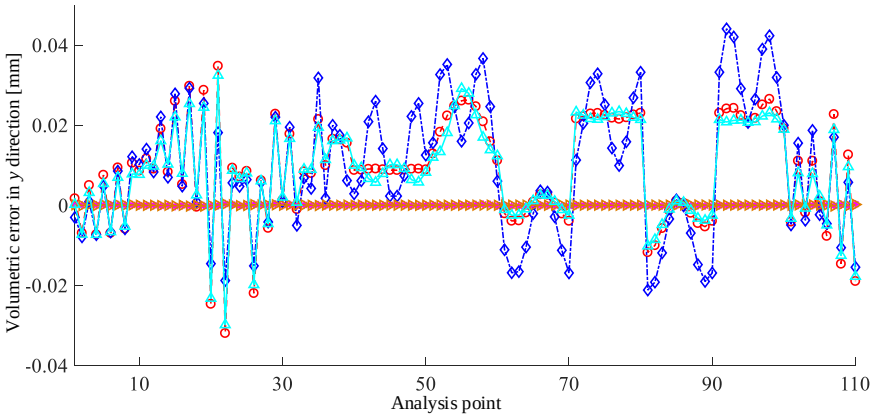
The actual cutter location can be calculated by substituting corresponding geometric errors and corresponding motion commands into Equation (17). Ideal motion commands and compensated motion commands were adopted, respectively. Deviation between the planned cutter location and the calculated cutter location is defined as the volumetric error. The simulated volumetric position errors in x, y and z direction that with total geometric error compensation, with sensitive geometric error compensation and without error compensation are displayed in Figure 11.

It can be found that the compensation of sensitive geometric errors in x direction can reduce the volumetric position errors in x direction to the results of total error compensation. Differently, the compensation of sensitive geometric error in y and z direction cannot reduce the volumetric position errors in x direction, illustrated in Figure 11. Therefore, the identification results of sensitive geometric errors in the corresponding identification direction are effective and correct. Similar conclusions can be obtained in the y and z direction.

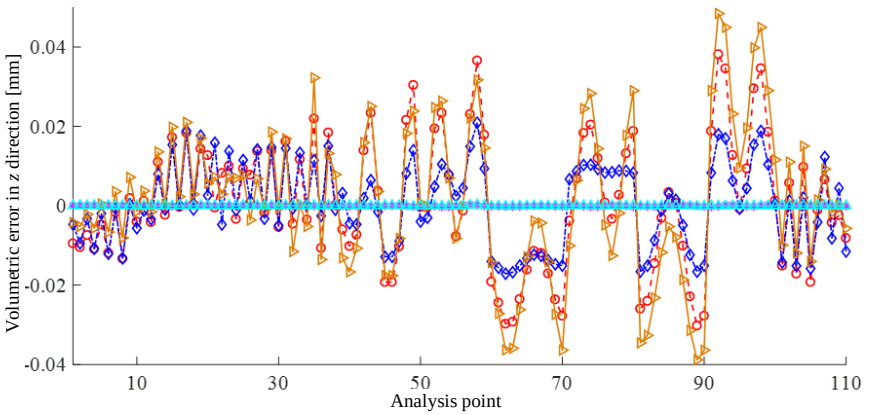
It is worth noting that the angular errors $\Delta\alpha(Z)$ $\Delta\beta(Z)$ and $\Delta\gamma(Z)$ cannot be compensated by using the existing linear axes. Hence, the corresponding angular errors should be paid the most attention during the design and assembling. In summary, the identification results of sensitive geometric errors in the x, y, and z direction based on the mapping table are effective and correct. The mapping table of sensitive geometric errors can be widely utilized in the precision design and control of the remanufacturing process of three-axis machine tools.



(**a**) volumetric error in x direction



(**b**) volumetric error in y direction



(**c**) volumetric error in z direction

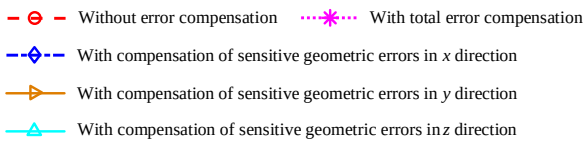
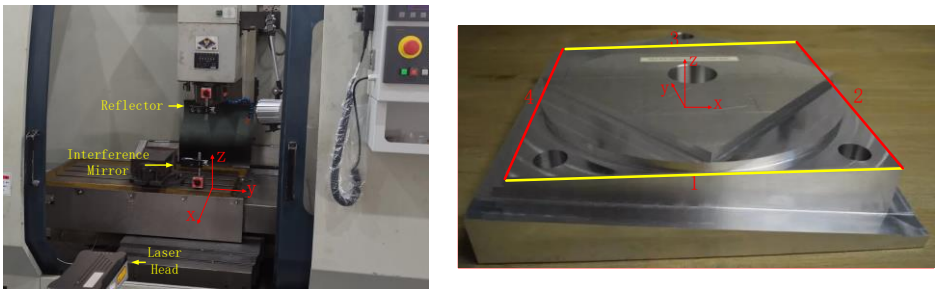


Figure 11. Comparison of simulation results.

5.3. Experimental Validation

To validate the simulation results, experiments of practical cutting with/without sensitive geometric error compensation are conducted on a remanufacturing three-axis machine MCV 850, with a SIEMENS 828D controller whose resolution is 1 µm.

Before cutting, 21 geometric errors of the machine tool are measured by the Renishaw laser interferometer XL-80 with nine-line method presented in [31]. The structure of the experimental machine is identical to the one of the simulation model shown in Figure 9. Figure 12a shows the experimental set-up for measuring by using the laser interferometer whose measurement accuracy is 0.5 µm. Sufficient warm-up time for the machine tool is needed before measuring. Let the spindle revolve at a normal speed and let the table and tool traverse the full measuring space for several hours. Table 6 shows the measured 21 geometric errors for the remanufacturing three-axis machine. The error values for any given point in the workspace can be calculated by linearly interpolating the values of the two neighboring errors which have already been measured. Then, the compensated NC data can be obtained according to Equation (18).



(**a**) (**b**)

Figure 12. Experimental set-up and test piece: (**a**) experimental set-up; and (**b**) the test piece.

A 6061 aluminum alloy NAS piece (see in Figure 12b) is machined by this machine tool. In the test piece, line 1 and line 3 are parallel, and line 2 and line 4 are parallel. The straightness errors of line 1 and 3 are prominently influenced by the volumetric position errors in y direction of the machine, and the straightness errors of line 2 and 4 are affected by the volumetric position errors in x direction of the machine. The length dimension of each line is 110 mm. As the tests are mainly for static/quasistatic error compensation, the feedrate of the experiments remains constant at 1 m/min. During experiments, an end mill of the radius 8 mm is used. The surface is finished under the spindle speed of 3000 rpm. The cutting depth is 0.5 mm. After the machining, the accuracy is inspected by a Hexagon Coordinate Measuring Machine (CMM), whose measurement accuracy is 1 µm.

Firstly, line 1 and 2 are machined without compensation of sensitive geometric errors, and then line 3 and 4 are machined with compensation of sensitive geometric errors in x and y directions. The straightness errors of line 1 and line 2 are 0.015 mm and 0.018 mm, respectively, and the straightness errors of line 3 and line 4 are 0.010 mm and 0.011 mm, respectively. Since during experiments, the feedrate is constant, so the dynamic error can be ignored. Before measuring and cutting, the machine has reached thermal balance, so the thermal error can be neglected. Therefore, the accuracy of machined workpiece is improved by the compensation of sensitive geometric errors. The remaining errors after compensation are mainly the vibration errors and servo errors, which are not considered in this study. These results indicate the effectiveness of the structural mapping law of sensitive geometric errors.

Table 6. Measured 21 geometric errors.

X/Y/Z Position (mm)	0	11	22	33	44	55	66	77	88	99	110
$\Delta x(X)$ (μm)	−0.5	1	2.5	3.5	5	6	8	9	11	13	15
$\Delta y(X)$ (μm)	2	2.5	2.5	0.5	−1.5	−2	−2	−1	1	3	3
$\Delta z(X)$ (μm)	3	3	0	−1	−1	−2	−1	−0.5	0	1	1
$\Delta\alpha(X)$ (s)	−0.5	1	2	2.5	3	4	4	5	6	6.5	7
$\Delta\beta(X)$ (s)	0.5	1.5	2.5	4	5	6.5	6	7	7.5	6	5.5
$\Delta\gamma(X)$ (s)	0.5	1	2	3.5	4.5	6	6.5	6	6	6.5	6.5
$\Delta x(Y)$ (μm)	0	0.5	1	0.5	0	0.5	0.5	0	1	0.5	0
$\Delta y(Y)$ (μm)	−3.5	−7	−7	−7	−9	−7	−5	−1	3	5	5
$\Delta z(Y)$ (μm)	−0.5	0	1	5	1	0	−0.5	0	0.5	1	3
$\Delta\alpha(Y)$ (s)	−0.5	0	1	2	3	3.5	4.5	5	6	6	6
$\Delta\beta(Y)$ (s)	1.5	3.5	5.5	6.5	8	9	9	9	7.5	7.5	7.5
$\Delta\gamma(Y)$ (s)	0	1	3	4	5	6	8	9	9	10	11
$\Delta x(Z)$ (μm)	−3	−1	1	2	1	0	1	1	0	−1	−2
$\Delta y(Z)$ (μm)	2	−10	2	4	3	2	2	0	0	−1	−3
$\Delta z(Z)$ (μm)	−4	−2.5	6	−0.5	2	−1.5	−0.5	−3.5	1.5	2.5	−3.5
$\Delta\alpha(Z)$ (s)	0.5	1.5	1.5	3	4	3	4	3	4	4	5
$\Delta\beta(Z)$ (s)	−1.5	−2	2.5	−2.5	−2.5	−1.5	−1.5	−1.5	−0.5	0.5	1
$\Delta\gamma(Z)$ (s)	0	0	0	0	0	0	0	0	0	0	0
$\Delta\gamma_{xy}$ (s)	5										
$\Delta\beta_{xz}$ (s)	−22.5										
$\Delta\alpha_{yz}$ (s)	45.5										

6. Conclusions

A quick identification method of sensitive geometric errors based on the structural mapping laws was proposed for the remanufacturing of three-axis milling machine tools. The sensitive geometric errors can be identified conveniently by looking up the mapping tables of volumetric position error and posture error, respectively. The contributions can be concluded as follows:

(1) Based on the proposed method, sensitive geometric error terms of different three-axis machine structures can be obtained without geometric error modeling and sensitivity analysis.
(2) The weak coupling relationship among the geometric errors of three-axis machine tools can be concluded, and the partial differential method was utilized to analyze the sensitivity of geometric errors.
(3) Mapping tables between the sensitive geometric errors and the machine tool structure can be applied to the convenient identification of sensitive error terms without professional knowledge.
(4) The identification results of sensitive geometric errors by using the proposed method are verified through simulation and experiment. The results showed that the straightness error of milling was improved up to 0.007 mm by compensating the identified sensitive geometric errors.

The sensitive geometric error terms of a three-axis machine tool can be quickly found out through the mapping table presented in this paper. The proposed mapping table is convenient and effective. However, the mapping laws are only verified for the orthogonal three-axis machine tools, the non-orthogonal machine tools will be studied in the

future. Meanwhile, the quantization sensitivity of geometric errors cannot be determined intuitively by using the method in this paper, which deserves further research.

Author Contributions: Conceptualization, W.D. and S.D.; methodology, S.D.; software, Z.S.; validation, Z.S.; formal analysis, S.D.; investigation, W.D.; resources, S.D.; data curation, Z.S.; writing—original draft preparation, W.D.; writing—review and editing, W.D. and S.D.; visualization, Z.S.; supervision, S.D.; project administration, S.D.; funding acquisition, S.D. All authors have read and agreed to the published version of the manuscript.

Funding: This research was funded by National Natural Science Foundation of China (Grant No. 51905470) and China Postdoctoral Science Foundation (No. 2020M671617).

Data Availability Statement: The data underlying this article will be shared upon reasonable request to the corresponding author.

Conflicts of Interest: The authors declare no conflict of interest.

References

1. Du, Y.; He, G.; Li, B.; Zhou, Z.; Wu, G. In service machine tool remanufacturing: A sustainable resource saving and high valued recovery approach. *Environ. Dev. Sustain.* **2022**, *24*, 1335–1358. [CrossRef]
2. Song, Z.Q.; Ding, S.; Chen, Z.W.; Lu, Z.W.; Wang, Z.Z. High-efficient calculation method for sensitive PDGEs of five-axis reconfigurable machine tool. *Machines* **2021**, *9*, 84. [CrossRef]
3. Fu, G.Q.; Fu, J.Z.; Xu, Y.T.; Chen, Z.C.; Lai, J.T. Accuracy enhancement of five-axis machine tool based on differential motion matrix: Geometric error modeling, identification and compensation. *Int. J. Mach. Tools Manuf.* **2015**, *89*, 170–181. [CrossRef]
4. Yang, J.X.; Ding, H. A new position independent geometric errors identification model of five-axis serial machine tools based on differential motion matrices. *Int. J. Mach. Tools Manuf.* **2016**, *104*, 68–77. [CrossRef]
5. Chen, G.H.; Zhang, L.; Wang, C.; Xiang, H.; Tong, G.Q.; Zhao, D.Z. High-precision modeling of CNCs' spatial errors based on screw theory. *SN Appl. Sci.* **2022**, *4*, 45. [CrossRef]
6. Zhong, X.M.; Liu, H.Q.; Mao, X.Y.; Li, B.; He, S.P.; Peng, F.Y. Volumetric error modeling, identification and compensation based on screw theory for a large multi-axis propeller-measuring machine. *Meas. Sci. Technol.* **2018**, *29*, 055011. [CrossRef]
7. Cheng, Q.; Feng, Q.N.; Liu, Z.F.; Gu, P.H.; Cai, L.G. Fluctuation prediction of machining accuracy for multi-axis machine tool based on stochastic process theory. *Proc. Inst. Mech. Eng. Part. C J. Mech. Eng. Sci.* **2015**, *229*, 2534–2550. [CrossRef]
8. Tao, H.F.; Chen, R.; Xuan, J.P.; Xia, Q.; Yang, Z.Y.; Zhang, X.; He, S.; Shi, T.L. Prioritization analysis and compensation of geometric errors for ultra-precision lathe based on the random forest methodology. *Precis. Eng.* **2020**, *61*, 23–40. [CrossRef]
9. Zhou, B.C.; Wang, S.L.; Fang, C.G.; Sun, S.L.; Dai, H. Geometric error modeling and compensation for five-axis CNC gear profile grinding machine tools. *Int. J. Adv. Manuf. Technol.* **2017**, *92*, 2639–2652. [CrossRef]
10. Ding, S.; Huang, X.D.; Yu, C.J.; Wang, W. Actual inverse kinematics for position-independent and position-dependent geometric error compensation of five-axis machine tools. *Int. J. Mach. Tools Manuf.* **2016**, *111*, 55–62. [CrossRef]
11. Wu, H.R.; Zheng, H.L.; Wang, W.K.; Xiang, X.P.; Rong, M.L. A method for tracing key geometric errors of vertical machining center based on global sensitivity analysis. *Int. J. Adv. Manuf. Technol.* **2020**, *106*, 3943–3956. [CrossRef]
12. Niu, P.; Cheng, Q.; Liu, Z.F.; Chu, H.Y. A machining accuracy improvement approach for a horizontal machining center based on analysis of geometric error characteristics. *Int. J. Adv. Manuf. Technol.* **2021**, *112*, 2873–2887. [CrossRef]
13. Li, J.; Xie, F.G.; Liu, X.J. Geometric error modeling and sensitivity analysis of a five-axis machine tool. *Int. J. Adv. Manuf. Technol.* **2016**, *82*, 2037–2051. [CrossRef]
14. Li, Q.Z.; Wang, W.; Jiang, Y.F.; Li, H.; Zhang, J.; Jiang, Z. A sensitivity method to analyze the volumetric error of five-axis machine tool. *Int. J. Adv. Manuf. Technol.* **2018**, *98*, 1791–1805. [CrossRef]
15. Li, D.X.; Feng, P.F.; Zhang, J.F.; Yu, D.W.; Wu, Z.J. An identification method for key geometric errors of machine tool based on matrix differential and experimental test. *Proc. Inst. Mech. Eng. Part. C J. Mech. Eng. Sci.* **2014**, *228*, 3141–3155. [CrossRef]
16. Cheng, Q.; Liu, G.B.; Liu, Z.F.; Xuan, D.S.; Chang, W.F. An identification approach for key geometric error sources of machine tool based on sensitivity analysis. *J. Mech. Eng.* **2012**, *48*, 171–179. (In Chinese) [CrossRef]
17. Cheng, Q.; Zhao, H.W.; Zhang, G.J.; Gu, P.H.; Cai, L.G. An analytical approach for crucial geometric errors identification of multi-axis machine tool based on global sensitivity analysis. *Int. J. Adv. Manuf. Technol.* **2014**, *75*, 107–121. [CrossRef]
18. Tian, W.J.; Liu, S.P.; Liu, X.X. Accuracy design of high precision machine tools using error sensitivity analysis methodology. *Proc. Inst. Mech. Eng. Part. C J. Mech. Eng. Sci.* **2017**, *231*, 3401–3413. [CrossRef]
19. Liu, X.J.; Wang, Y.; Qiu, L.M.; Wu, C.R.; Zhang, P.; Zhang, S.Y. An improved geometric error analysis method considering the variety of sensitivities over working space. *Adv. Mech. Eng.* **2018**, *10*, 1–12. [CrossRef]
20. Fan, J.W.; Tao, H.H.; Wu, C.J.; Tang, Y.H. Method of error sensitivity analysis of machine tools. *J. Beijing Univ. Technol.* **2019**, *45*, 314–321. (In Chinese)
21. Fan, J.W.; Tao, H.H.; Pan, R.; Chen, D.J. An approach for accuracy enhancement of five-axis machine tools based on quantitative interval sensitivity analysis. *Mech. Mach. Theory* **2020**, *148*, 103806. [CrossRef]

22. Fan, J.W.; Wang, P.T.; Ren, X.F. A novel global sensitivity analysis method for vital geometric errors of five-axis machine tools. *Int. J. Adv. Manuf. Technol.* **2021**, *117*, 3515–3527. [CrossRef]
23. Guo, S.J.; Jiang, G.D.; Mei, X.S. Investigation of sensitivity analysis and compensation parameter optimization of geometric error for five-axis machine tool. *Int. J. Adv. Manuf. Technol.* **2017**, *93*, 3229–3243. [CrossRef]
24. Guo, S.J.; Zhang, D.S. Geometric Error Analysis and Compensation of Rotary Axes of Five-axis Machine Tools. *Adv. Eng. Sci.* **2020**, *52*, 130–139. (In Chinese)
25. Xia, C.J.; Wang, S.L.; Sun, S.L.; Lin, X.C.; Huang, X.D. Geometric error to tooth surface error model and identification of crucial errors in five-axis CNC gear profile grinding machines. *Comput. Integr. Manuf. Syst.* **2020**, *26*, 1191–1201. (In Chinese)
26. Li, P.Z.; Zhao, R.H.; Luo, L. A geometric accuracy error analysis method for turn-milling combined NC machine tool. *Symmetry* **2020**, *12*, 1622. [CrossRef]
27. Zou, X.C.; Zhao, X.S.; Wang, Z.W.; Li, G.; Hu, Z.J.; Sun, T. Error distribution of a 5-Axis measuring machine based on sensitivity analysis of geometric errors. *Math. Probl. Eng.* **2020**, *2020*, 8146975. [CrossRef]
28. Tang, H.; Duan, J.A.; Lan, S.H.; Shui, H.Y. A new geometric error modeling approach for multi-axis system based on stream of variation theory. *Int. J. Mach. Tools Manuf.* **2015**, *92*, 41–51. [CrossRef]
29. Fu, G.Q.; Rao, Y.J.; Xie, Y.P.; Gao, H.L.; Deng, X.L. Error sensitivity analysis of motion axis for five-axis CNC machine tools with geometric error contribution. *China Mech. Eng.* **2020**, *31*, 1518–1528. (In Chinese)
30. Jiang, X.G.; Cui, Z.W.; Wang, L.; Liu, C.; Li, M.J.; Liu, J.; Du, Y. Critical geometric errors identification of a five-axis machine tool based on global quantitative sensitivity analysis. *Int. J. Adv. Manuf. Technol.* **2022**, *119*, 3717–3727. [CrossRef]
31. Dai, K.; Zhang, S.; Shu, Y.; Zhang, W.; Zhang, Z. Modified identification method of geometric error for translational axis of CNC machine tools. *Comput. Integr. Manuf. Syst.* **2021**, *27*, 1319–1327. (In Chinese)